ELSEVIER

Contents lists available at ScienceDirect

European Journal of Pharmaceutical Sciences

journal homepage: www.elsevier.com/locate/ejps





Small molecules modified mesoporous silica nanoparticles orally deliver indomethacin with synergistic effect

Shiliang Yin ^a, Lin Cai ^a, Xuan Li ^a, Kai Lin ^a, Xianbao Shi ^b, Hong Zhang ^c, Lijie Wang ^a, Jing Li ^{a,*}

- a School of Pharmacy, Shenyang Medical College, 146 Huanghe North Street, Shenyang, Liaoning, China
- ^b Department of Pharmacy, the First Affiliated Hospital of Jinzhou Medical University, Jinzhou, China
- ^c School of Lifescience and Biopharmaceutics, Shenyang Pharmaceutical University, Shenyang, Liaoning, China

ARTICLE INFO

Keywords: Small molecules modified mesoporous silica nanoparticles

Anti-inflammatory

ABSTRACT

Molecularly functional drug delivery systems possessed huge potentials to realize novel drug administration. To explore small molecules modified drug delivery, a series of small molecules modified mesoporous silica nanoparticles (L-Mal-MSNs, D-Mal-MSNs) were established by grafting small molecules. Poorly water-soluble indomethacin (IMC) was chosen to load into these small molecules modified carriers as well as corresponding control carrier, and further to study characteristics and delivery effects of drug loaded carriers. The results indicated that all these small molecules modified carriers formed hydrogen bonds with drugs and can successfully convert drug crystal phase to amorphous state so as to enhance drug dissolution compared to raw drug. *In vivo* rat intestinal perfusion demonstrated that IMC loaded L-Mal-MSNs performed the fastest drug absorption while analgesic and anti-inflammatory effects of IMC loaded D-Mal-MSNs turned out to be the best, giving hints that D-malic acid exhibited best synergic functions for IMC. The herein small molecules modified delivery system is an effective solution strategy for the current application of analgesia and anti-inflammatory drugs with outstanding significance.

1. Introduction

Inflammation is defined as the resistance of the vascular defence response tissue in the organism to the cumulative damage of inflammatory factors. Therefore, inflammation can lead to many diseases, such as osteoarthritis (OA) and inflammatory bowel disease (IBD), etc. OA is the most common type of arthritis, which can occur in all major joints of the body such as knee joint and elbow joint, and even cause disability in severe cases. It is known as the "deathless cancer" (Quicke et al., 2022; Sanchez-Lopez et al., 2022). It can be seen that inflammation has become the top "killer" of national health. Currently, the most widely used non-steroidal anti-inflammatory drugs in patients with inflammation, such as ibuprofen, flubiprofen, diclofenac, celeoxib, indomethacin, meloxicam, piroxicam and naproxen, are effective in inhibiting inflammation, pain and joint stiffness, and slowing or preventing disease progression. However, long-term use of these drugs may result in unintended accumulation of non-target organs, tissues or cells and lead to toxic effects resulting in serious adverse reactions. In addition, most anti-inflammatory drugs are dissoluble and their oral bioavailability is limited (Zhou et al., 2018). Therefore, urgent development of specific,

effective and safe drugs has important clinical significance.

At the site of inflammation, inflammatory mediators are released after activation of inflammatory cells, resulting in increased local vascular permeability, plasma exosmosis and edema. At the same time, metabolic activity of cells at the site of inflammation increases, leading to hypoxia and inducing anaerobic glycolysis and lactation transition. Currently, 14 biomarkers related to acute inflammation have been identified, including lactic acid, malic acid, citric acid, tartaric acid, trans dehydroandrosterone, aldosterone, etc. (Zhang et al., 2015; Lee et al., 2019; Hernandez-Baixauli et al., 2022). Malic acid, for example, has anti-oxidation and anti-fatigue effects. Related studies have shown that L-malic acid has recognition and induction effect because of its chiral structure. It can inhibit the cycle progression of HaCaT cells in G0/G1 and have anti-proliferation effect. On the other hand, adding malic acid to a drug can increase its stability and promote the absorption and diffusion of the drug through tissues. L-malic acid can also improve the anti-inflammatory and antioxidant capacity of jejunum, improve digestion and absorption function, affect barrier function, and thus improve intestinal health. At present, there are a large number of studies and noteworthy reports on the anti-inflammatory effects of malic acid

E-mail address: dddefghijklmn@163.com (J. Li).

^{*} Corresponding author.

and other inflammatory biomarkers. However, few studies have reported on linking inflammatory biomarkers to drug carriers to improve the anti-inflammatory efficacy of drugs. Therefore, in this study, inflammatory biomarkers (represented by malic acid and tartaric acid) were connected to the carrier to construct a new "pre-carrier". The grafted biomarkers fell off after targeted delivery, giving full play to the anti-inflammatory effect of synergistic drugs, and the two sides were combined to cause the rapid destruction of inflammatory lesions, creating an efficient drug delivery system for inflammation treatment.

Nanomaterials can effectively solve the damage to non-target organs, showing significant advantages in targeting, immunogenicity, biocompatibility and other aspects (Hartwig et al., 2021; Bannister et al., 2020; Xu et al., 2022; Li et al., 2023; Zhang et al., 2023; Li et al., 2023). With the development of nanotechnology, materials developed on the nanoscale have attracted more and more attention in the fields of drug delivery, diagnosis, medical imaging and engineering, and are mainly applied in the treatment of diseases such as tumor and inflammation (Chagri et al., 2022). Among all available nanomaterials, many studies have been conducted on mesoporous silica nanoparticles due to their unique properties: (1) large specific surface area and pore volume provide great potential for adsorption and loading of drugs in pores; (2) Excellent mesoporous structure and adjustable pore size enable better control of drug load and release;(3) Easily modified surfaces for controlled and targeted drug delivery enhance therapeutic efficacy and reduce toxicity; (4) The biosafety evaluation of cytotoxicity, biodegradation, distribution and excretion in vivo has obtained satisfactory results; (5) Combinations with magnetic and/or luminescent compounds allow simultaneous drug delivery and bioimaging; (6) Excellent surface properties and porosity can be used as candidate materials for bone regeneration bioactive materials (Vallet-Regi et al., 2022; Feng et al., 2023; Shah et al., 2022; Vallet-Regí et al., 2022; Djayanti et al., 2023; Carvalho et al., 2022). Based on the above unique advantages (Yang et al., 2022; Pan et al., 2021), mesoporous silica nanoparticles have become a research hotspot in the field of medicine.

Surface modified mesoporous silica nanoparticles have been widely studied in recent years since surface modification provides vital advantages for achieving specific aims (Michailidis et al., 2017; Kankala et al., 2020; Heydari et al., 2023). To explore contributions of chiral small molecules modified mesoporous silica nanoparticle for anti-inflammatory drug delivery, the present paper constructed small molecules modified mesoporous silica nanoparticle indomethacin (IMC) delivery system using chiral malic acid grafted silica, which was different from current studies with chiral tartaric acid (Liu et al., 2021; Gou et al., 2021). The herein drug delivery system developed by this project, which integrates targeting, anti-inflammatory effect and drug bioavailability enhancement, is an effective solution strategy for the current application of anti-inflammatory drugs, which has important significance.

2. Materials and methods

2.1. Materials

L-malic acid (\geq 99%), D-malic acid (\geq 99%), 3-ammonia propyl triethoxy silane (APTES, \geq 99%), cetyltrimethyl ammonium bromide (CTAB, \geq 99%), indomethacin (IMC, \geq 99%), tetraethoxysilane (TEOS, \geq 99%) were purchased from Dalian Meilun Biological Co., Ltd (China). Other chemical reagents are reagent grade, purchased from Tianjin Damao Chemical Reagent Factory (Tianjin, China). Deionized water was prepared by ion exchange method. All animal experiments in this study were conducted according to the Guidelines for the Care and Use of Laboratory Animals that was authorized by the Ethics Review Committee for Animal Experimentation of Shenyang Pharmaceutical University (Shenyang, Liaoning, China).

2.2. Synthesis of L-Mal-MSNs, D-Mal-MSNs and blank MSNs

The preparation method of L-Mal-MSNs and D-Mal-MSNs was as follows. In the first step, chiral malic acid (L-Mal and D-Mal) was reacted with silane coupling agent (APTES) to synthesize chiral silane coupling agent (L-Mal-APTES and D-Mal-APTES). Next, 1.2 g L-malic acid or Dmalic acid was weighed and dissolved in 80 ml anhydrous ethanol under stirring on 60°C water bath. Afterwards, 2 ml APTES was added and stirred continuously for 4 h before stopping to collect the white precipitate. The above precipitates were washed with anhydrous ethanol, centrifuged and dried to obtain chiral silane coupling agents (L-Mal-APTES and D-Mal-APTES). In the second step, small molecules modified mesoporous silica nanoparticles were synthesized. In detail, 1.50 g of CTAB was weighed and added to a mixture of 160 ml redistilled water and 48 ml anhydrous ethanol. Under the condition of 25°C water bath, 1.4 ml ammonia water and 1.00 g chiral silane coupling agent were added to the above solution in sequence. 4 ml TEOS was gradually dropped into the solution under intense stirring. After 4 h, the agitation was stopped and left for 24 h before centrifugation. The precipitates obtained after centrifugation were washed twice with water and ethanol respectively and dried in a 45°C oven. The dried precipitate was placed in 200 ml 0.01 mol/L HCl-methanol solution and refluxed for 12 h. After reflux, the mixture was centrifuged, washed and dried to obtain small molecules modified mesoporous silica nanoparticles (L-Mal-MSNS and D-Mal-MSNS). Blank MSNs was prepared in almost the same way as previous steps without adding chiral silane coupling agents in the second step (Wu et al., 2020).

2.3. Porous structure

Morphology of L-Mal-MSNs, D-Mal-MSNs, blank MSNs were characterized using SURA 35-field emission scanning electron microscope (ZEISS, Germany). The sample was pasted on a metal cylinder and sputtered with gold under vacuum. Nitrogen adsorption/desorption of L-Mal-MSNs, D-Mal-MSNs, blank MSNs, were determined by V-sorb 4800P (app-one, China). All samples were vacuum dried and degassed at 80°C to remove residual moisture.

2.4. Drug loading process

A certain amount of IMC was placed in L-Mal-MSNs, D-Mal-MSNs and blank MSNs by the adsorption drug loading method. The acetone solution of IMC (20 mg/ml) was obtained by placing 20 mg IMC in 1 ml acetone. After complete dissolution of IMC, 60 mg carrier (L-Mal-MSNs D-Mal-MSNs, blank MSNs were added into the drug solution to obtain a mixed solution (mass ratio of drug to carrier 1:3). The mixture was stirred overnight at room temperature. After the stirring was completed, the mixture was dried in a vacuum drying oven at 40°C. The dried precipitated product was washed with a pH 7.4 phosphate buffer solution to remove the unloaded drug to obtain IMC loaded blank MSNs, IMC loaded L-Mal-MSNs, IMC loaded D-Mal-MSNs. The drug loading capacity can be determined by accurately weighing the mass of drug loaded carrier. Under ultrasonic, the loaded IMC was completely extracted with methanol, and finally drug content was measured at 318 nm by UV-2600 (Shimazu, Japan), and the absorbance was measured three times and the average value was calculated.

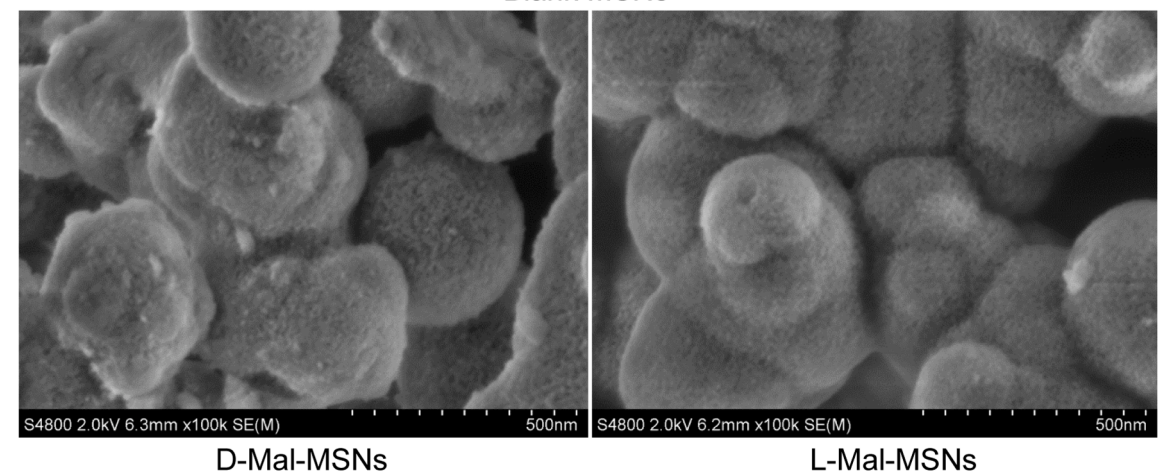
$$Drugloading capacity(\%) = (W_{drugin carrier} / W_{drugloaded carrier}) \times 100$$

2.5. Fourier transform infrared spectroscopy (FTIR)

FTIR (FTIR-650, Gangdong, Tianjin, China) was used to obtain spectra in the spectral region of $400-4000~{\rm cm}^{-1}$. Drug, carriers, and drug loaded carriers were measured by drying each sample and pressing into tables with KBr.

Α

Blank MSNs



В

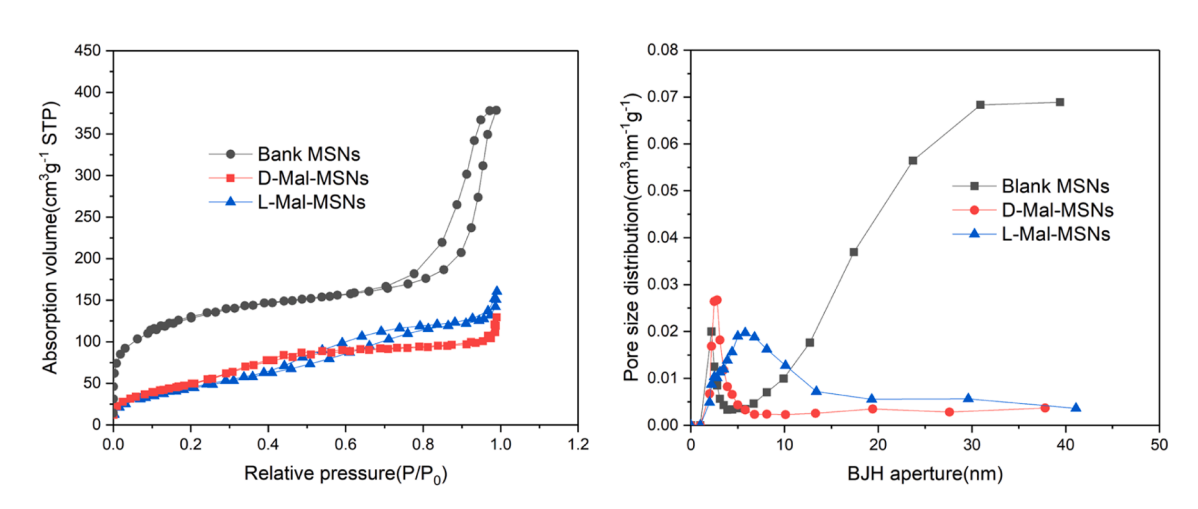


Fig. 1. A, SEM images of L-Mal-MSNs, D-Mal-MSNs and blank MSNs; B, nitrogen desorption diagram and pore size distribution diagram of L-Mal-MSNs, D-Mal-MSNs and blank MSNs.

2.6. Differential scanning calorimeter (DSC)

The heat flow diagrams of drug, drug loaded carriers were measured by DSC (HSC-4, Hengjiu, Beijing, China). The sample was placed in an aluminum dish and heated from 25°C to 200°C at a rate of 5°C/min . Before measuring, samples were dried in vacuum oven to remove

 $residue\ moisture\ completely.$

2.7. Drug release in vitro

The paddle method (50 rpm, 37° C) was used with 200 ml pH 6.8 phosphate buffer solution as dissolution medium, and the test was

carried out on RC806D dissolution tester. 5 mg drug or drug loaded carrier containing 5 mg IMC was precisely weighed and put into 200 ml of dissolution medium respectively. At predetermined time points (5 min, 10 min, 15 min, 20 min, 30 min, 40 min, 1 h, 1.5 h, 2 h, 3 h, 4 h, 6 h, 8 h), 5 ml sample was withdrawn and after each sampling, 5 ml of dissolution medium at 37°C was replenished to maintain a constant volume. After the sample was filtered through a 0.45 μm water-based microporous membrane, UV-2600 was used to measure the absorbance at a wavelength of 320 nm to calculate the cumulative release amount and draw dissolution curves.

2.8. In vivo rat intestinal perfusion

Twelve Wistar male rats weighing 200 ± 20 g were randomly divided into four groups on average, named IMC, IMC loaded blank MSNs, IMC loaded L-Mal-MSNs, IMC loaded D-Mal-MSNs. 1.35 mg IMC or drug loaded carrier containing 1.35 mg IMC was weighed, and added to 300 ml of Krebs-Ringer buffer (K-R buffer) containing 50 mg of phenol red respectively to prepare the test solution. Before the experiment, the rats were fasted (normal drinking water) for 12 h, anesthetized (20% urethane 5ml/kg), and fixed. The abdominal cavity was incised along the abdominal midline of the rat, and a small slit was cut at the upper and lower ends of the duodenum, and the cannula was fixed to obtain a rat model. The thermostatic peristaltic pump was connected to the rat model, then peristaltic pump was turned on to equilibrate at a constant flow rate (5 ml/min) for 10 min, and then perfuse at 2.5 ml/min. At the

predetermined time points (0 h, 0.25 h, 0.5 h, 0.75 h, 1 h, 1.5 h, 2 h, 2.5 h, 3 h), 3 ml of samples were taken out, and after each sampling, 3 ml of Krebs-Ringer buffer containing phenol red was added. The experiment was stopped after the constant temperature peristaltic pump circulated for 3 h (Xiao-Ying et al., 2019). The peak area of drug was measured with HPLC (Waters e2695), and the absorbance of phenol red was measured with UV-2600. After the sample was filtered by microporous membrane, 0.3 ml sample was added into 3 ml sodium hydroxide solution, and the content of phenol red was determined at 558 nm.

HPLC analysis working conditions were as follows. Chromatographic column: C_{18} (5 microns, 4.6×250 mm), mobile phase: acetonitrile: 0.1 mol/L acetic acid (70:30, v/v), column temperature: 30° C, analytical wavelength: 228 nm, velocity: 1.0 ml/min. The absorption rate constant (K_{a}) was calculated for each trial.

2.9. In vivo pharmacodynamic studies

2.9.1. Hot plate analgesia test

Fifty KM mice were randomly divided into model group (normal saline), IMC group (100mg/kg), IMC loaded L-Mal-MSNs group, IMC loaded D-Mal-MSNs group, IMC loaded blank MSNs group. The drug was administered continuously for 7 days. After the last dose, adjusted the water bath to 55°C. The mice were then placed on a hot plate and the time was counted when they were placed on the hot plate. The day before the formal test, the pain response time of mice should be detected in advance, and the mice with pain response time between 10-30s were

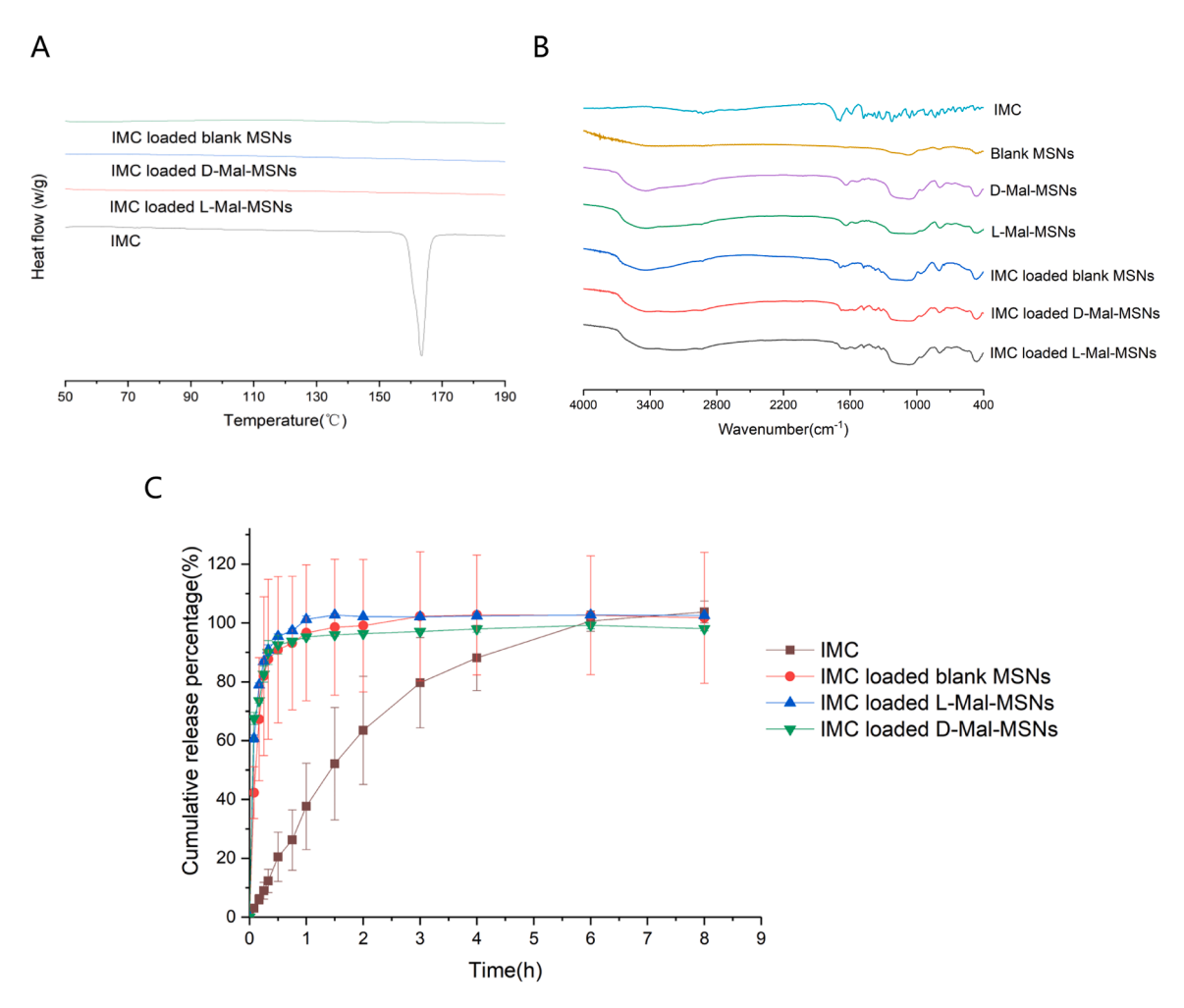


Fig. 2. A, DSC diagram of IMC, IMC loaded L-Mal-MSNs, IMC loaded D-Mal-MSNs and IMC loaded blank MSNs; B, FTIR curves of IMC, L-Mal-MSNs, D-Mal-MSNs, blank MSNs, IMC loaded L-Mal-MSNs, IMC loaded D-Mal-MSNs and IMC loaded blank MSNs; C, Cumulative drug release *in vitro* of IMC, IMC loaded L-Mal-MSNs, IMC loaded D-Mal-MSNs and IMC loaded blank MSNs.

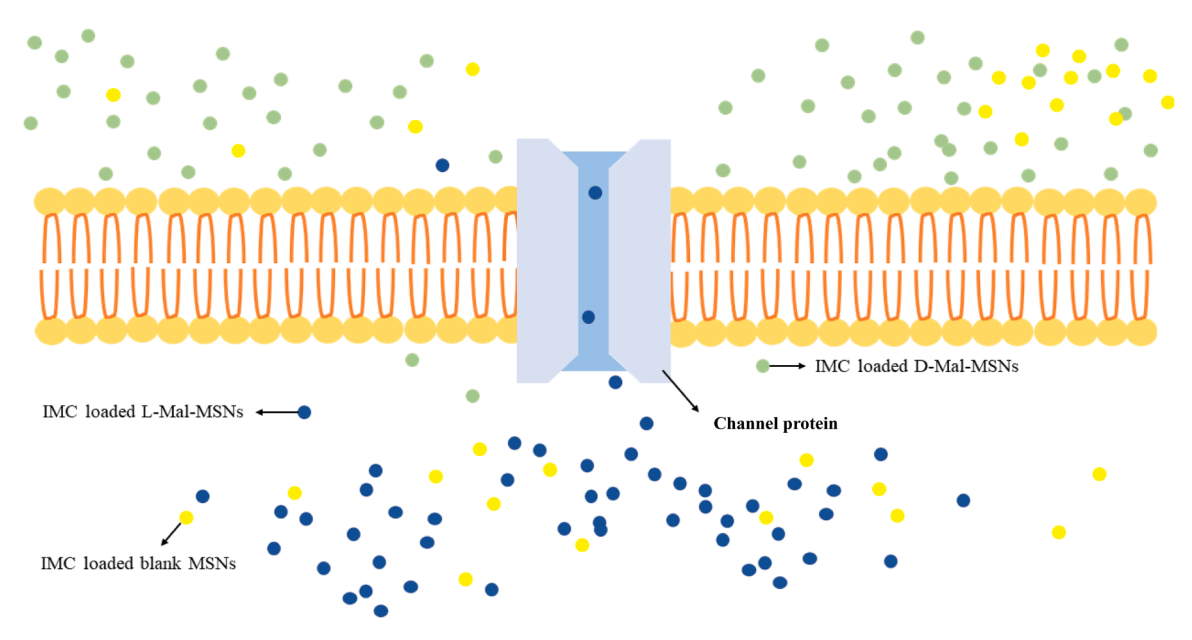


Fig. 3. Schematic diagram of drug loaded carrier absorption in intestinal transmembrane.

qualified. The normal pain response time (post-licking foot) of qualified rats was measured twice, each time with an interval of 5min. The average value was calculated as the pain threshold before administration. On the test day, pain response time was measured at 30min, 60min, 90min, 120min, 180min, 240min and 360min after administration.

2.9.2. Acetic acid twisting experiment

Fifty healthy KM mice (18-22g) were randomly divided into model group (normal saline), IMC group (100mg/kg), IMC loaded L-Mal-MSNs group (100mg/kg), IMC loaded D-Mal-MSNs group (100mg/kg), IMC loaded blank MSNs group (100mg/kg). The drug was administered continuously for 7 days. 0.6% acetic acid solution was prepared in advance and preheated with 37°C water bath. On the test day, 0.2ml/piece of 0.6% acetic acid solution preheated at 37°C was injected intraperitoneally 30 min after the last administration. The time (latent period) and the number of writhing reaction were observed and recorded within 20 min. Stimulation of the peritoneum caused a lasting pain response, resulting in a twisted body reaction in mice. Writhing reaction was based on the behavior criteria of abdominal contraction and concave, extension of hind limbs, hip elevation and peristaltic crawling of mice. In this study, Oneway ANOVA and Dunnet's t test were used for statistical significance difference analysis (SPSS19.0 version).

2.9.3. Mouse ear swelling induced by xylene

Fifty healthy KM mice (18-22g) were randomly divided into model group (normal saline), IMC group (100mg/kg), IMC loaded L-Mal-MSNs group (100mg/kg), IMC loaded D-Mal-MSNs group (100mg/kg), IMC loaded blank MSNs group (100mg/kg). 1h after the last administration, xylene 0.05 ml was applied to the right ear of mice in each group. 30 min later, the mice were sacrificed for cervical dislocation. Ear slices of the same area were placed on the same part of both ears with a 6 mm perforator and weighed with an electronic balance. Swelling degree and inhibition rate were calculated.

Rightearswelling(mg) = Rightearweight(mg) - Leftearweight(mg)

The paraffin blocks were cut into $5\mu m$ thick sections and stained with hematoxylin-eosin (HE). The pathological changes of ear tissues, including the degree of epidermal and dermal edema and lymphocyte infiltration, were observed under an optical microscope. Mouse eyeballs were taken for 1.0 ml of blood, and centrifuged at $3000 \, r/min$ for $10 \, min$ after natural coagulation. Serum was taken out and placed in EP tube and stored in refrigerator at -20°C for later use. Serum values of IL-1 β and TNF- α were determined by ELISA according to the instructions of the kit. In this study, Oneway ANOVA and Dunnet's t test were used for statistical significance difference analysis (SPSS19.0 version).

3. Results

3.1. Characteristics of small molecularly modified mesoporous silica nanoparticles

According to SEM images (Fig. 1A), blank MSNs were spherical nanoparticles with rough surface with diameter of about 100 nm. On the contrary, L-Mal-MSNs and D-Mal-MSNs were nanoparticles with irregular morphology of spherical or rodlike with diameter in the range of 200 nm to 500 nm after small molecular modification. According to Fig. 1B, nitrogen adsorption/desorption isotherms belonged to type IV, indicating that L-Mal-MSNs, D-Mal-MSNs and blank MSNs all had mesopores. The specific surface area of blank MSNs was 458.16 $\rm m^2/g$ and pore volume was 0.451 $\rm cm^3/g$, which were bigger than L-Mal-MSNs (specific surface area of 168.46 $\rm m^2/g$, pore volume of 0.250 $\rm cm^3/g$) and D-Mal-MSNs (specific surface area of 184.38 $\rm m^2/g$, pore volume of 0.197 $\rm cm^3/g$), demonstrating that small molecular modification significantly lowered specific surface area and pore volume.

3.2. Characterizations after drug loading

Drug loading capacity of IMC loaded D-Mal-MSNS (12.64%) and IMC loaded L-Mal-MSNS (10.57%) was higher than that IMC loaded blank MSNs (8.94%). It was obvious that the larger pore diameter of L-Mal-MSNs and D-Mal-MSNs contributed to its higher drug loading capacity

Table 1

Analgesic response time of mice after orally administered different samples.

| Sample | 0 min | 15 min | 30 min | 45 min | 60 min | 75 min | 90 min |
|-----------------------|------------------|-------------------|------------------|--------------------|------------------|------------------|------------------|
| Model | 12.73 ± 3.63 | $12.25{\pm}1.95$ | $13.35{\pm}2.19$ | 9.99±1.30 | 13.76 ± 2.15 | 15.19±4.59 | 13.67±2.60 |
| IMC loaded blank MSNs | 14.21 ± 2.33 | 16.19±5.34* | 14.08 ± 4.27 | 13.39 ± 4.46 | $13.19{\pm}1.35$ | 14.43 ± 3.19 | 15.79 ± 5.76 |
| IMC loaded D-Mal-MSNs | $11.89{\pm}1.77$ | 15.96 ± 4.54 | 13.66 ± 3.98 | 17.84±5.59** | 14.04 ± 7.10 | 15.95 ± 8.27 | 14.79 ± 4.50 |
| IMC loaded L-Mal-MSNs | $12.56{\pm}2.71$ | 17.03±3.48* | 16.56±5.97* | 13.28±3.12* | 16.39±4.62* | $15.82{\pm}6.77$ | 15.90 ± 5.69 |
| IMC | 14.58 ± 4.14 | $18.84{\pm}5.88*$ | 15.75 ± 5.70 | $14.26 {\pm} 4.66$ | $13.28{\pm}2.54$ | $11.03{\pm}1.80$ | 14.25 ± 4.94 |

^{**}p<0.01; ***p<0.001 v.s. Model

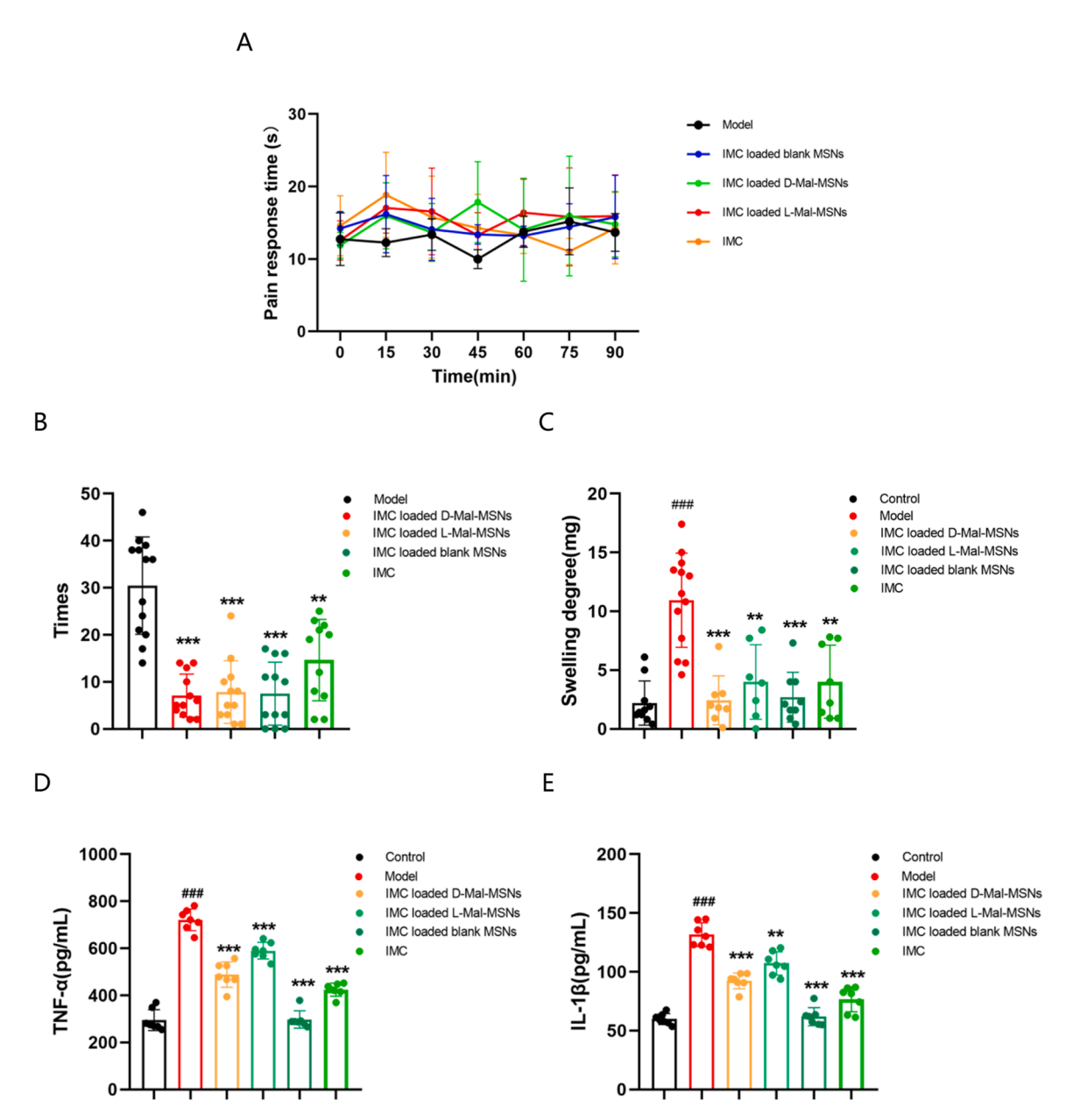


Fig. 4. A, analgesic response time of mice after orally administered different samples; B, writhing times of mice after orally administered different samples; C, ear swelling degree (%) of mice after orally administered different samples; D, Concentration of TNF- α in serum of mice in xylene-induced ear swelling model; E, Concentration of IL-1 β in serum of mice in xylene-induced ear swelling model.

compared with blank MSNs. As shown in the Fig. 2A, an endothermic peak appeared in the IMC heat flow diagram at 163.5° C, which was basically consistent with the melting point temperature of IMC. As the synthesis method of L-Mal-MSNs and D-Mal-MSNs was similar, L-Mal-MSNs was taken as an example. The FTIR diagram (Fig. 2B) of L-Mal-MSNs showed that the antisymmetric stretching vibration absorption

peak of Si-O-Si bond located at 1076.0 cm $^{-1}$, the symmetric stretching vibration absorption peak of Si-O-Si bond was at 790.6 cm $^{-1}$, and the bending vibration absorption peak of Si-O bond located at 460.9 cm $^{-1}$. The stretching vibration absorption peak of carbonyl of amide was at 1639.1cm $^{-1}$ and -OH was at 3434.6 cm $^{-1}$, indicating that L-Mal-MSNs successfully achieved small molecularly modification. Further, IMC

Table 2Writhing times of mice after orally administered different samples.

| Sample | Model (times) | IMC loaded D-Mal- MSNs (times) | IMC loaded L-Mal- MSNs (times) | IMC (times) | IMC loaded blank MSNs (times) |
|----------------|---|---|---|------------------|-------------------------------------|
| Twisting times | $\begin{array}{c} 30.46 \\ \pm 10.35 \end{array}$ | 7.08 ±4.54*** | 7.83 ±6.63*** | 14.64 ±8.65** | 7.50 ±6.71*** |

^{**} *p*<0.01;

Table 3The swelling degree of the mouse ear caused by xylene.

| Sample | Left ear wt. (mg) | Right ear wt. (mg) | Swelling degree (mg) | Inhibitory rate(%) |
|---------------------------|----------------------|-----------------------|-------------------------------|--------------------|
| Control | 12.35 ± 1.58 | 14.55±2.51 | 2.2±1.87 | - |
| Model | 9.91±2.09 | 20.85±3.34 | 10.94 ±4.00 ^{###} | - |
| IMC loaded D- Mal-MSNs | 9.15±1.08 | 11.58 ± 2.45 | 2.43±2.08*** | 77.83 |
| IMC loaded L- Mal-MSNs | $9.49{\pm}2.17$ | 13.47±3.25 | 3.99±3.17** | 63.56 |
| IMC | $8.51 {\pm} 0.98$ | 12.53 ± 3.11 | 4.01±3.11** | 63.32 |
| IMC loaded blank MSNs | 8.76±1.20 | 11.44±1.92 | 2.69±2.12*** | 75.42 |

^{###} p<0.001 v.s. Control;

loaded blank MSNs, IMC loaded L-Mal-MSNs and IMC loaded D-Mal-MSNs presented similar result, so IMC loaded L-Mal-MSNS was discussed as an example. In the FTIR diagram of IMC, the two spectral peaks at 1589.0 cm⁻¹ and 1479 cm⁻¹ were the skeleton stretching vibration absorption peak of benzene ring in IMC structure, the characteristic absorption peak at 833.0 cm⁻¹ was the para-position substitution of benzene ring, 1713.4 cm⁻¹ was the C=O stretching vibration absorption peak of carboxylic acid, and 1690.9 cm⁻¹ was the C=O stretching vibration absorption peak of amide (Gou et al., 2021). However, in the FTIR diagram of IMC loaded L-Mal-MSNs, the absorption peak of benzene ring almost disappeared, and the stretching vibration absorption peak of C=O of carboxylic acid and amide moved to a low wave number (red shift), indicating that IMC formed a hydrogen bond with L-Mal-MSNs.

3.3. Drug release in vitro

As shown in Fig. 2C, the drug release rate of three drug loaded carriers were superior to IMC, indicating that the three carriers can improve drug release because all drug remained amorphous state in carriers according to DSC results. Moreover, release rate and maximum release amount of IMC loaded blank MSNs, IMC loaded L-Mal-MSNs and IMC loaded D-Mal-MSNs were similar, further confirming the above *in vitro* release analysis that poorly water-soluble drug release was not determined by porous structure parameters of carriers when small molecules modified mesoporous silica nanoparticle was applied as drug carrier.

 Table 4

 Inflammatory markers in serum after ear swelling experiment.

| Sample | Control | Model | IMC loaded D-Mal-MSNs | IMC loaded L-Mal-MSNs | IMC | IMC loaded blank MSNs |
|--------|--------------|---|-----------------------|-----------------------|-----------------|-----------------------|
| TNF-α | 295.33±44.61 | $721.37 \pm 45.60^{\#\#}$ $131.68 \pm 10.12^{\#\#\#}$ | 488.11±53.93*** | 589.84±35.55*** | 421.10±27.71*** | 297.24±37.07*** |
| IL-1β | 59.91±4.66 | | 92.25±6.70*** | 107.22±9.92** | 76.64±10.62*** | 61.95±7.71*** |

^{###} p<0.001 v.s. Control;

3.4. In vivo rate intestinal perfusion

The absorption rate constant of IMC loaded L-Mal-MSNs was the largest among IMC (Ka: 5.24×10^{-4}), IMC loaded blank MSNs (Ka: 5.35×10^{-4}), IMC loaded L-Mal-MSNs (Ka: 6.43×10^{-4}) and IMC loaded D-Mal-MSNs (Ka: 2.36×10^{-4}). Since blank MSNs, L-Mal-MSNs and IMC loaded D-Mal-MSNs were nanoparticles that can pass through small intestinal epithelial cells (see Fig. 3), and in vitro drug release result was different from in vivo rate intestinal result, indicating that their ability to deliver drugs through small intestinal epithelial cells turned out to be the crucial step for oral administration.

3.5. In vivo pharmacodynamic studies

The hot plate analgesia results were shown Table 1 and Fig. 4A. Compared with model group, IMC loaded blank MSNs, IMC loaded L-Mal-MSNs, IMC loaded D-Mal-MSNs, and IMC showed significant central analgesic effects (*p < 0.05;**p < 0.01v.s. Model). Moreover, IMC loaded blank MSNs, IMC loaded L-Mal-MSNs and IMC exerted the fastest effect, showing significant analgesic effects 15 min after administration, which was in agreement with in vivo rate intestinal perfusion result that the absorption rate constant of IMC loaded L-Mal-MSNs, IMC loaded blank MSNs and IMC loaded L-Mal-MSNs were higher than IMC loaded D-Mal-MSNs. To further confirm analgesic effect of small molecules modified mesoporous silica nanoparticles drug delivery system, the acetic acid writhing analgesia results were displayed in Table 2 and Fig. 4B. Compared with model group, IMC loaded blank MSNs, IMC loaded L-Mal-MSNs, IMC loaded D-Mal-MSNs, and IMC could significantly reduce the twisting times of mice in acetic acid twisting experiment (**p < 0.01;***p < 0.001 v.s. Model), that is, all the above drugs had significant analgesic effects, and IMC loaded D-Mal-MSNs presented the best efficacy.

Anti-inflammatory test of small molecules modified mesoporous silica nanoparticles drug delivery system was studied using the ear swelling anti-inflammatory test, and these results were shown in Table 3 and Fig. 4C. It was obvious that compared with the control group, the swelling degree of ear piece of mice in the model group was significantly increased (###p < 0.001), indicating that the model was successfully established. It demonstrated that single administration of IMC loaded blank MSNs, IMC loaded L-Mal-MSNs, IMC loaded D-Mal-MSNs, and IMC could reduce the degree of ear swelling induced by xylene (**p < 0.01;***p < 0.001 v.s.Model), showing their significant antiinflammatory effects. Furthermore, representative inflammatory factor of TNF- α and IL-1 β (pleas see Table 4) were analyzed after ear swelling anti-inflammatory study. According to Fig. 4 D and E, the concentrations of TNF- α and IL-1 β in the model group were significantly increased (###p<0.001), indicating that the inflammation model of ear swelling in xylene mice was successfully established. Compared with model group, single administration of IMC loaded blank MSNs, IMC loaded L-Mal-MSNs, IMC loaded D-Mal-MSNs, and IMC significantly decreased serum concentrations of TNF- α and IL-1 β (**p<0.01;***p<0.001), revealing their significant anti-inflammatory effects. Pathological section images of ear swelling experiment were presented in Fig. 5. Compared with the control group, the ear slices of mice in the model group showed subcutaneous soft tissue congestion, edema, and scattered inflammatory cell infiltration. The model of ear swelling induced by

^{***} p<0.001 v.s. Model

^{**} p<0.01;

^{***} p<0.001 v.s. Model

^{**} *p*<0.01;

^{***} p<0.001 v.s. Model

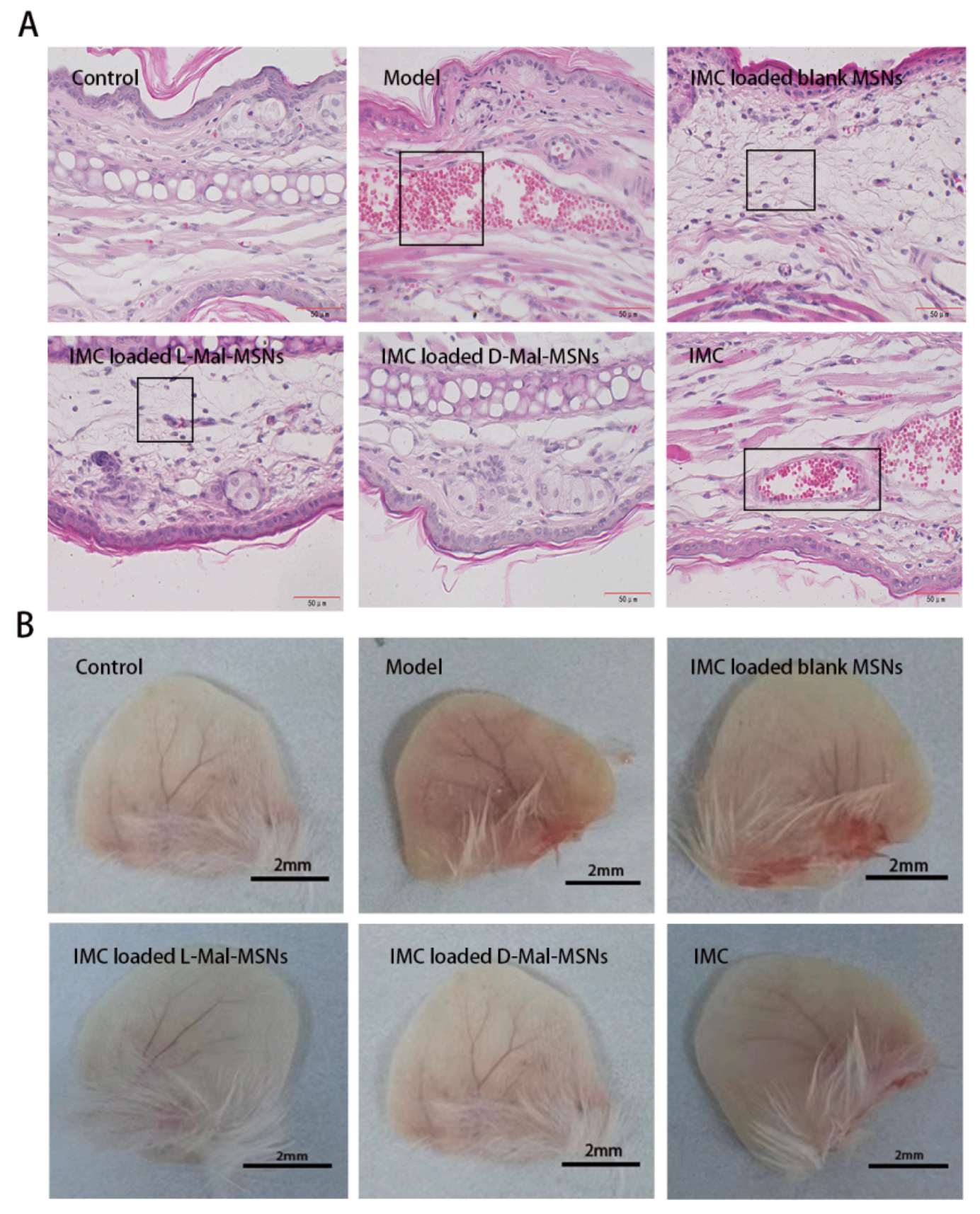


Fig. 5. Ear slice of xylene induced ear swelling model mice of different samples.

xylene was established successfully. Compared with ear tablets in model group, administration of IMC loaded blank MSNs, IMC loaded L-Mal-MSNs, IMC loaded D-Mal-MSNs, and IMC can significantly relieve edema and inflammatory infiltration caused by xylene.

4. Discussion

4.1. Characteristics of small molecularly modified mesoporous silica nanoparticles

It was obvious that particle diameter was significantly enlarged for small molecules modified mesoporous silica nanoparticles after grafting small molecules in the silica frame. Since the part grafted on the surface of nanoparticles was small molecule, there were no significant differences in the surface morphology of L-type MSNs and D-type MSNs. It was predicted that it was needed to have nanoparticles instead of disordered mesoporous silica because surface modification effect may be better after grafting molecules onto nanoparticles due to larger surface area of nanoparticles than particles. Furthermore, both L-Mal-MSNs and D-Mal-MSNs presented irregular shape, and chiral malic acid disturbed the order of silica condensation owing to its large molecule. Pore diameters of L-Mal-MSNs and D-Mal-MSNs were a little bigger than blank MSNs (pore diameter of L-Mal-MSNs was almost 240% of blank MSNs, D-Mal-MSNs was about 120% of blank MSNs), possibly because the introduction of malic acid modified silane coupling agent enlarged the size of micelle template formed by CTAB owing to its electric charge.

4.2. Drug loading abilities

Blank MSNs, L-Mal-MSNs and D-Mal-MSNs had no obvious endothermic peak, indicating that they were in an amorphous state. IMC loaded blank MSNs, IMC loaded L-Mal-MSNs and IMC loaded D-Mal-MSNs showed no obvious endothermic peak, indicating that IMC was successfully loaded into the pores of mesoporous silica nanoparticles and existed in an amorphous state (Wang et al., 2019a; Wang et al., 2019b; Liu et al., 2021). Though specific surface area and pore volume of L-Mal-MSNs and D-Mal-MSNs were lower than blank MSNs, IMC loaded L-Mal-MSNs and IMC loaded D-Mal-MSNs obtained similar release effects compared to blank MSNs because small molecules modified mesoporous silica nanoparticles loaded larger amount of amorphous drug than mesoporous silica. The reason can be ascribed that stronger hydrogen bonds formed by carboxyl groups of small molecules and amino groups of drug than hydrogen bonds formed between hydroxyl groups of mesoporous silica and amino groups of drug.

4.3. In vivo drug delivery effects

According to in vivo absorption rate result, since the chemical configurations of amino acids constituting proteins were mostly L-type, it was speculated that the channel proteins of mucosal cells preferred to absorb L-type drug carriers. The in vivo intestinal drug absorption result of L-Mal-MSNs and D-Mal-MSNs demonstrated that L-type chiral mesoporous silica nanoparticles performed faster delivery rate than D-type. Among IMC loaded blank MSNs, IMC loaded L-Mal-MSNs and IMC, analgesic effect of IMC loaded L-Mal-MSNs performed longest analgesic duration, indicating that IMC loaded L-Mal-MSNs with the highest in vivo absorption rate contributed to obtain better analgesic effect. However, the analgesic effect of IMC loaded D-Mal-MSNs with the longest analgesic duration at 45 min after administration (**p<0.01v.s.Model) reflected that D-Mal-MSNs orally delivered IMC with lowest in vivo absorption rate but the best analgesic effect. Since silica degraded in biological environment (He et al., 2009; He et al., 2008), the above result gave hints that D-malic acid that fell off from degraded silica frame exhibited best synergic analgesia function for IMC.

Among these, IMC loaded D-Mal-MSNs exerted the highest swelling inhibition rate to present the strongest anti-swelling and anti-

inflammatory effect, which was in agreement with the above analgesia results. Furthermore, representative inflammatory factor of TNF- α and IL-1 β were analyzed after ear swelling anti-inflammatory study. The levels of TNF- α and IL-1 β in serum of IMC loaded D-Mal-MSNs group were lower than those of IMC loaded L-Mal-MSNs group, indicating that IMC loaded D-Mal-MSNs had better anti-inflammatory effect. Mice ear tablets with IMC loaded blank MSNs and IMC loaded L-Mal-MSNs still had subcutaneous soft tissue edema, but no inflammatory cell infiltration. There was no subcutaneous soft tissue edema and inflammatory cell infiltration in IMC loaded D-Mal-MSNs group. However, there was still congestion and edema in the IMC group, but no inflammatory cell infiltration. These results suggest that IMC loaded blank MSNs, IMC loaded L-Mal-MSNs, IMC loaded D-Mal-MSNs all have significant anti-inflammatory effects, among which IMC loaded D-Mal-MSNs performed the best anti-inflammatory effect.

5. Conclusion

The present small molecules modified mesoporous silica nanoparticles belonged to nanoparticles with mesopores and malic acids. Though the internal and outside grafted malic acids lowered specific surface area and pore volume, their pore diameter was not influenced. Herein, IMC loaded L-Mal-MSNs, IMC loaded D-Mal-MSNs and IMC loaded blank MSNs can successfully convert IMC crystal state to amorphous phase and IMC formed hydrogen bond forces with these three carriers. Drug release rate of the three drug loaded carriers were obviously faster than IMC, indicating that the three carriers can improve drug release because all drug remained amorphous state in carriers according to DSC results. The in vivo intestinal drug absorption result indicated that L-Mal-MSNs performed faster drug absorption rate than D-Mal-MSNs. However, analgesic and anti-inflammatory effects of IMC loaded D-Mal-MSNs turned out to be the best, giving hints that D-malic acid exhibited best synergic analgesia function for IMC. It is believed that the present small molecules modified mesoporous silica nanoparticles can perform synergistic effect to enhance analgesia and antiinflammatory effects.

CRediT authorship contribution statement

Shiliang Yin: Investigation. Lin Cai: Methodology. Xuan Li: Formal analysis. Kai Lin: Data curation. Xianbao Shi: Formal analysis. Hong Zhang: Methodology. Lijie Wang: Software. Jing Li: Writing – original draft.

Declaration of competing interest

No.

Data availability

Data will be made available on request.

Acknowledgements

This work was supported by National Natural Science Foundation of China (no. 82104114), Shenyang Young and middle-aged scientific and technological innovation talent support program from Shenyang Bureau of Science and Technology (no. RC220022), General project of Natural Science Foundation of Liaoning Province from Department of Science & Technology of Liaoning Province (2021-MS-350).

References

Bannister, A.H., Bromma, K., Sung, W., Monica, M., Cicon, L., Howard, P., Chow, R.L., Schuemann, J., Chithrani, D.B., 2020. Modulation of nanoparticle uptake,

- intracellular distribution, and retention with docetaxel to enhance radiotherapy. Br. J. Radiol. 93, 1106.
- Carvalho, G.C., Marena, G.D., Karnopp, J.C.F., Jorge, J., Sábio, R.M., Martines, M.A.U., Bauab, T.M., Chorilli, M., 2022. Cetyltrimethylammonium bromide in the synthesis of mesoporous silica nanoparticles: general aspects and *in vitro* toxicity. Adv. Colloid Interface Sci. 307, 102746.
- Chagri, S., Ng, D.Y.W., Weil, T., 2022. Designing bioresponsive nanomaterials for intracellular self-assembly. Nature 6, 320–338.
- Djayanti, K., Maharjan, P., Cho, K.H., Jeong, S., Kim, M.S., Shin, M.C., Min, K.A., 2023. Mesoporous silica nanoparticles as a potential nanoplatform: therapeutic applications and considerations. Int. J. Mol. Sci. 24 (7), 6349.
- Feng, Y., Liao, Z., Li, M., Zhang, H., Li, T., Qin, X., Li, S., Wu, C., You, F., Liao, X., Cai, L., Yang, H., Liu, Y., 2023. Mesoporous silica nanoparticles-based nanoplatforms: basic construction, current state, and emerging applications in anticancer therapeutics. Adv. Healthc. Mater. 12, 2201884.
- Gou, K., Wang, Y., Guo, X., Wang, Y., Bian, Y., Zhao, H., Guo, Y., Pang, Y., Xie, L., Li, S., Li, H., 2021. Carboxyl-functionalized mesoporous silica nanoparticles for the controlled delivery of poorly water-soluble non-steroidal anti-inflammatory drugs. Acta Biomater. 134, 576–592.
- Hartwig, O., Boushehri, M.S., Shalaby, KS., Loretz, B., Lamprecht, A., Lehr, C.M., 2021. Drug delivery to the inflamed intestinal mucosa-targeting technologies and human cell culture models for better therapies of IBD. Adv. Drug Deliv. Rev. 175, 113828.
- He, Q., Zhang, Z., Gao, Yu, Shi, J., Li, Y., 2009. Intracellular localization and cytotoxicity of spherical mesoporous silica nano-and microparticles. Small 5, 2722–2729.
- He, X., Nie, H., Wang, K., Tan, W., Wu, Xu, Zhang, P., 2008. In vivo study of biodistribution and urinary excretion of surface-modified silica nanoparticles. Anal. Chem. 80, 9597–9603.
- Hernandez-Baixauli, J., Abasolo, N., Palacios-Jordan, H., Foguet-Romero, E., Suñol, D., Galofré, M., Caimari, A., Baselga-Escudero, L., Del Bas, J.M., Mulero, M., 2022. Imbalances in TCA, short fatty acids and one-carbon metabolisms as important features of homeostatic disruption evidenced by a multi-omics integrative approach of LPS-induced chronic inflammation in male wistar rats. Int. J. Mol. Sci. 23, 2563.
- Heydari, S.R., Ghahremani, M.H., Atyabi, F., Bafkary, R., Jaafari, M.R., Dinarvand, R., 2023. Aptamer-modified chitosan-capped mesoporous silica nanoparticles for codelivery of cytarabine and daunorubicin in leukemia. Int. J. Pharm. 646, 123495.
- Kankala, R.K., Han, Y.H., Na, J., Lee, C.H., Sun, Z., Wang, S.B., Kimura, T., Ok, Y.S., Yamauchi, Y., Chen, A.Z., Wu, K.C., 2020. Nanoarchitectured structure and surface biofunctionality of mesoporous silica nanoparticles. Adv. Mater. 32 (23), 1907035.
- Lee, B., Heo, J., Hong, S.Y., Kim, E.Y., Sohn, Y.J., Jung, H.S., 2019. DL-Malic acid as a component of α-hydroxy acids: effect on 2,4-dinitrochlorobenzene-induced inflammation in atopic dermatitis-like skin lesions in vitro and in vivo. Immunopharmacol. Immunotoxicol. 41, 614–621.
- Li, H., Gou, Ř., Liao, J., Wang, Y., Qu, R., Tang, Q., Gan, J., Zou, L., Shi, S., 2023. Recent advances in nano-targeting drug delivery systems for rheumatoid arthritis treatment. Acta Mater. Med. 2 (1), 23–41.
- Li, X., Wang, H., Chen, Y., et al., 2023. Novel emerging nano-assisted anti-cancer strategies based on the STING pathway. Acta Mater. Med. 2 (3), 323–341.
- Liu, R., Wang, X., Fan, Na, Song, H., Ma, P., Li, C., Li, J., Sun, J., 2021. Superiority of Chiral-handed mesoporous silica nanoparticles in delivering Nimesulide. Mater. Sci. Eng. B Adv. Funct. Solid State Mater. 269, 115161.

- Michailidis, M., Sorzabal-Bellido, I., Adamidou, E.A., Diaz-Fernandez, Y.A., Aveyard, J., Wengier, R., Grigoriev, D., Raval, R., Benayahu, Y., D'Sa, R.A., Shchukin, D., 2017. Modified mesoporous silica nanoparticles with a dual synergetic antibacterial effect. ACS Appl. Mater. Interfaces 9 (44), 38364–38372.
- Pan, P., Yue, Q., Yang, X., Ren, Y., Alharthi, F.A., Alghamdi, A., Su, J., Deng, Y., 2021. Structure engineering of yolk-shell magnetic mesoporous silica microspheres with broccoli-like morphology for efficient catalysis and enhanced cellular uptake. Small. 17, 2006925.
- Quicke, J.G., Conaghan, P.G., Corp, N., Peat, G., 2022. Osteoarthritis year in review 2021: epidemiology & therapy. Osteoarthr. Cartil. 30, 196–206.
- Sanchez-Lopez, E., Coras, R., Torres, A., Lane, N.E., Guma, M., 2022. Synovial inflammation in osteoarthritis progression. Nat. Rev. Rheumatol. 18, 258–275
- Shah, S., Famta, P., Bagasariya, D., Charankumar, K., Sikder, A., Kashikar, R., Kotha, AK., Chougule, M.B., Khatri, D.K., Asthana, A., Raghuvanshi, R.S., Singh, S.B., Srivastava, S., 2022. Tuning mesoporous silica nanoparticles in novel avenues of cancer therapy. Mol. Pharm. 19 (12), 4428–4452.
- Vallet-Regí, M., Schüth, F., Lozano, D., Colilla, M., Manzano, M., 2022. Engineering mesoporous silica nanoparticles for drug delivery: where are we after two decades? Chem. Soc. Rev. 51 (13), 5365–5451.
- Vallet-Regi, M.A., Schuth, F., Lozano, D., Colilla, M., Manzano, M., 2022. Engineering mesoporous silica nanoparticles for drug delivery: where are we after two decades? Chem. Soc. Rev. 51, 13.
- Wang, J., Ke, J., Wang, Y., Wu, X., Li, H., Xu, L., 2019b. Improvement on the drug dissolution of diazepaam by using chiral mesoporous silica. Pract. Pharm. Clin. Remedies 22, 1299–1302.
- Wang, X., Li, C., Fan, Na, Li, J., Zhang, H., Shang, L., He, Z., Sun, J., 2019a. Amino functionalized chiral mesoporous silica nanoparticles for improved loading and release of poorly water-soluble drug. Asian J. Pharm. Sci. 14, 405–412.
- Wu, L., Gou, K., Guo, X., Guo, Y., Li, H., 2020. Dual response to pH and chiral microenvironments for the release of a flurbiprofen-loaded chiral self-assembled mesoporous silica drug delivery system. Colloids Surf. B Biointerfaces 199, 111501.
- Xiao-Ying, W., Hong, L., Xiao-Yi, Z.W., Wen, M., Wei, H.Y., 2019. Intestinal absorption of phenolic acids in Rhus chinensis extracts by in situ single-pass perfusion model in rats. China J. Chin. Mater. Med. 44, 2373–2378.
- Xu, X., Li, R., Dong, R., Yang, Y., Wang, H., Cheng, J., Liu, Y., Ye, J., 2022. In vitro characterization and cellular uptake profiles of TAMs-targeted lipid calcium carbonate nanoparticles for cancer immunotherapy. Acta Mater. Med. 1 (3), 400–410
- Yang, Y., Chen, F., Xu, N., Yao, Q., Wang, R., Xie, X., Zhang, F., He, Y., Shao, D., Dong, W., Fan, J., Sun, W., Peng, X., 2022. Red-light-triggered self-destructive mesoporous silica nanoparticles for cascade-amplifying chemo-photodynamic therapy favoring antitumor immune responses. Biomaterials 281, 121368.
- Zhang, C., Zuo, Y., Zhang, T., et al., 2023. Advances in nanoscale carrier-based approaches to reduce toxicity and enhance efficacy of podophyllotoxin. Acta Mater. Med. 2 (4), 430–448.
- Zhang, W., Hua, Y., Zhang, M., Ji, P., Li, J., Zhang, L., Li, P., Wei, Y., 2015. Metabonomic analysis of the anti-inflammatory effects of volatile oils of Angelica sinensis on rat model of acute inflammation. Biomed. Chromatogr. 29, 902–910.
- Zhou, J., Zhu, F., Li, J., Wang, Y., 2018. Concealed body mesoporous silica nanoparticles for orally delivering indometacin with chiral recognition function. Mater. Sci. Eng. C Mater. Biol. Appl. 90, 314–324.